applied sciences

MDPI

Article

Bond Graph-Based Approach to Modeling Variable-Speed Gearboxes with Multi-Type Clutches

Jiangming Wu [1,2], Hongzhi Yan [1,2,*], Shuangqi Liu [1,2], Yin Zhang [1,2] and Wuzhong Tan [1,3]

[1] School of Mechanical and Electrical Engineering, Central South University, Changsha 410083, China; wujm1919@csu.edu.cn (J.W.); liusqcsu@gmail.com (S.L.); zy20csu@gmail.com (Y.Z.); twzcsu@gmail.com (W.T.)
[2] The State Key Laboratory of High-Performance and Complex Manufacturing, Central South University, Changsha 410083, China
[3] AECC Hunan Aviation Powerplant Research Institute, Zhuzhou 412002, China
* Correspondence: yhzcsu@163.com

Abstract: The modeling and simulation of gearboxes is important for analyzing the dynamic characteristics and designing control strategies of transmission systems. Variable-speed gearboxes include compound planetary gear trains and clutches, which complicates dynamic modeling. Here, a procedural bond graph-based modeling method that considers many uncertainties is proposed. The proposed method yields a constant system–structure model. First, bond graph models of the two most common planetary gears were summarized, and were used as sub-models of a compound planetary gear train. Then, the Karnopp friction sub-model of the friction clutch and a relative angular displacement sub-model of the one-way clutch were constructed. Based on the dynamic coupling between the sub-models, the modeling steps of the gearbox, including the compound planetary gear train friction clutch one-way clutch coupling system, are described in detail. Next, the main sources of uncertainties of gearbox were analyzed and the simulation methods were given. Finally, the novel uncertain bond graph model was used to simulate the double planetary gearbox; the transmission ratio before and after the shift was 2.42 and 1.72, compared with the design values of 2.41 and 1.71, respectively; the deviation is within 5.8%; The average rotating speeds of the output shaft fluctuated by 6 and 2.5% respectively, which was within a reasonable range, so the effectiveness of the method is verified.

Keywords: planetary gear trains; clutch; gearbox; uncertain bond graph; dynamic system modeling

Citation: Wu, J.; Yan, H.; Liu, S.; Zhang, Y.; Tan, W. Bond Graph-Based Approach to Modeling Variable-Speed Gearboxes with Multi-Type Clutches. *Appl. Sci.* **2022**, *12*, 6181. https://doi.org/10.3390/app12126181

Academic Editor: Elisa Quintarelli

Received: 13 April 2022
Accepted: 14 June 2022
Published: 17 June 2022

1. Introduction

Gearbox modeling is an important step in the design process of transmission systems. By solving mathematical models, the system's dynamic characteristics can be analyzed prior to prototyping, and the gearbox dynamic response characteristics can be effectively predicted for given input conditions. Then, effective suggestions regarding the design and control of transmission systems can be provided [1].

The dynamic response of a typical transmission system is affected by many uncertain factors. No mathematical model can account for all factors that affect transmission systems [2]; adding more components to the model increases the modeling cost and the model's complexity, resulting in time-consuming calculations or difficult solutions. Therefore, from the perspective of the calculation cost reduction and improvement of the system's design efficiency, efficient and accurate modeling methods are necessary for designing and evaluating gearboxes.

Much research has been performed in the field of gearbox modeling and the dynamic response of gear trains. The Lagrange equation approach and the bond graph (BG) method [3] are common modeling techniques in the field of gear system modeling and simulation. When dealing with complex kinematic layouts, the BG model can intuitively represent the kinematic relationship between a system's parts, and an abstract dynamic

equation is obtained using Lagrange's law [4]. Based on the causal relationship between the components of a BG model, the algebraic relationship between the flow variables and potential variables can be inferred for obtaining dynamic model equations [5]. So far, bond graph theory is widely used in the analysis of a variety of engineering systems. Benjamin et al., used bond method to analyze the influence of different excitations on the vibration level of a helicopter's semi-active suspension [6]. Barjuei [7] constructed the bond graph model of an exoskeleton actuator and extended it to the dynamic modeling of all types of wearable robot actuators. In the research of modeling and Simulation of gear trains, for example, Deur [8,9] modeled a four-speed automatic transmission using the BG theory methods, and used it for analyzing the system response dynamics in the case of wheels, for fully applied brakes and for the brake-off scenario [10]. The shift of a 10-gear gearbox was analyzed in [11], and an extra clutch was utilized for improving the shifting performance using the BG theory methods. Ivanovic [12] proposed a method for transforming device-mapping BG models into conceptual torque-path BGs. The BG method was used in [13] for optimizing the double-transition shift control, and different control strategies were proposed. A systematic design method was explored in [14] for synthesizing the configuration schemes of multi-row and multi-speed AT based on the lever analogy. Li et al. [15] considered three subsystems: a planetary gear train (PGT), clutch, and inertia rotor, proposed a standardized modeling process, and verified the effectiveness of this method on example gearboxes. A wind turbine gearbox was modeled in [16] using the BG method, to develop a framework for transmission chain modeling, and the parameters were synthesized in Monte Carlo simulations. The transmission path of vibrations in aero-engines was analyzed in [17] using the BG theory methods, to efficiently diagnose and minimize noise and vibration in the design stage. Tan [18] discussed the effects of stiffness, damping, and inertia on the dynamic response of gear trains, based on the bond graph method.

The existing research mainly focuses on linear models and on the dynamic response analysis of gear trains. The influencing factors that are considered in these models are relatively few, and the proposed modeling methods have strict requirements for configuring gear trains; in addition, the guidance modeling process is not universal. Moreover, with the wide application of new-generation gearboxes, the engagement and disengagement of configured clutches yields variable model structures, which imposes limitations on dealing with this problem. Given the limited documentation and research in this field, this study proposes a general and efficient dynamic modeling method for a gearbox that includes a compound planetary–friction clutch—a one-way clutch.

The main objective of this paper was to present a modeling method for the uncBG model of a variable-speed gearbox with a friction clutch and a one-way clutch. To verify the effectiveness and rationality of this method, a double-row double planetary gearbox was used as an example for modeling and simulations.

The remainder of this paper is organized as follows. Section 2 introduces a double-row double planetary gearbox as the research object. In Section 3, the construction process of the BG models of two commonly used PGTs is presented. The friction clutch model and the one-way clutch model are introduced in Sections 4 and 5, respectively. Section 6 presents the coupling methods for the three basic models. Then, the main uncertainties of the system are analyzed, and the construction method of the uncertain BG (uncBG) model is presented in Section 7. Subsequently, in Section 8, the uncBG modeling method is used for simulating a two-gear gearbox, and the solution results are evaluated. Finally, the study conclusions are summarized.

2. Research Object

Taking a double-row double planetary gearbox as the research object, it can realize two gear speed output under the condition of constant input speed (high-speed transmission ratio: 1.71, low-speed transmission ratio: 2.41), which is commonly used in high-speed helicopter transmission systems. A one-way clutch was installed between the ring and

housing. The input and output ends of the friction clutch were integrated with the ring gear and housing, respectively, and a uniform load mechanism was arranged between the input shaft and the sun gear. The transmission system controlled the separation and engagement of the friction clutch by adjusting the hydraulic pressure, to realize the gear shift. Its three-dimensional diagram and structural schematic diagram are shown in Figure 1. R1, P1 and S respectively represent the ring gear, planetary gear and sun gear in the first PGT, R2 and P2 respectively represent the ring gear and planetary gear in the second PGT.

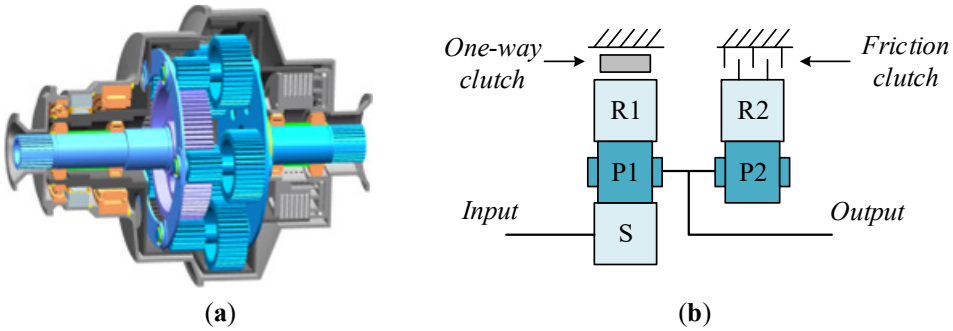

Figure 1. Double-row double planetary gearbox: (**a**) three-dimensional drawing, (**b**) structure diagram.

3. BG Models of PGTs

PGTs are characterized by high loads and large transmission ratios. A PGT can split power when transmitting it, and ensures that the input and output shafts are on the same horizontal line. Therefore, PGTs are used in most mechanical power transmission systems, such as automobiles, aerospace vehicles, and machine tools. The difficulty of PGT modeling is that the planetary gear rotates around the central gear with the star carrier. The BG method provides a reasonable method for PGT modeling [10]. Two commonly used PGT-based BG models are described below.

3.1. Single-Pinion PGT

The most common and widely used PGT has a single planetary gear transmission mechanism between the ring gear and the sun gear. The kinematic relationship between the single-pinion PGT (S-PGT) components is shown in Figure 2. The following relationship can be obtained by assuming equal linear velocities at the gear meshing point [13]:

$$\omega_p r_p = (\omega_c - \omega_s) r_s \tag{1}$$

$$\omega_p r_p = (\omega_r - \omega_c) r_r \tag{2}$$

the characteristic equation is

$$\omega_s - (\beta + 1)\omega_c + \beta\omega_r = 0 \tag{3}$$

Here, ω_p, ω_s, and ω_r are the rotation speeds of the planetary gear, the sun gear, and the ring gear, respectively. The parameters r_p, r_s, and r_r are the pitch radii of the planetary gear, the sun gear, and the ring gear, respectively. The parameter β is the PGT parameter, defined as $\beta = z_r/z_s$ (z_r: number of teeth of the ring gear; z_s: number of teeth of the sun gear). The kinematic relationship between the parts is fundamental for establishing the BG model. A good dynamic model of a PGT also should consider the effects of the gear moment of inertia, rotational damping, and meshing stiffness.

As shown in Figure 3, there are four one-nodes in the bonding diagram model of a single-pinion PGT, representing the sun gear, the planet carrier, the ring gear, and the planetary gear. An independent PGT cannot accomplish power transmission, and should be combined with input equipment (e.g., motor and engine), a clutch, and other components. Therefore, the sun gear, the ring gear, and the planetary carrier can be used as the input

components. The first three can be connected to an external system as an input or output power part; the key causality was not considered in the present study. The R and I elements on each one-node represent the rotational damping and the moment of inertia of the corresponding part, respectively; the 0-node represents the meshing point; finally, C on node 0 represents flexibility.

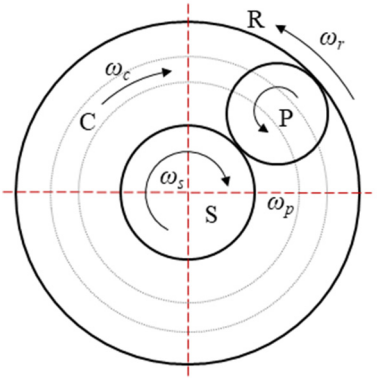

Figure 2. Kinematic diagram of the S-PGT.

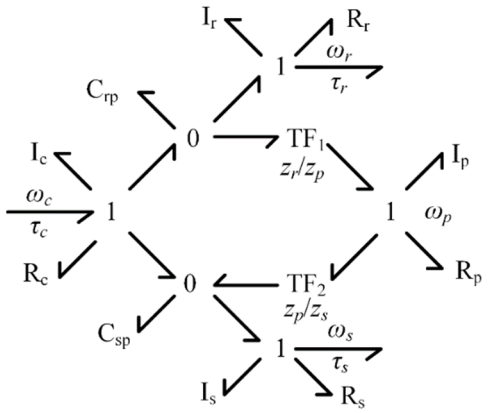

Figure 3. BG model of the S-PGT.

When the contact between gears is regarded as an elastic contact, the BG model features three energy-storage parameters. The parameter θ_{sp} is the relative angular displacement between the planet and the sun, while θ_{rp} is the relative angular displacement between the planet and ring. The parameters τ_s, τ_r, and τ_c are the torques of the sun gear, the ring gear, and the planetary carrier, respectively.

For node 1, the rotation speeds for all the keys are the same, and the algebraic sum of the torques is 0, as shown in Figure 3.

$$\dot{\theta}_{sp} = \omega_c - \omega_s + \omega_p \mathrm{TF}_2 \tag{4}$$

$$\dot{\theta}_{rp} = \omega_c - \omega_r - \omega_p {\mathrm{TF}_1}^{-1} \tag{5}$$

For node 0, the torques for all the keys are the same, and the algebraic sum of the rotation speeds is 0. The torque balance equation of the S-PGT is as follows:

$$\tau_s = \theta_{sp} C_{sp}^{-1} - I_s \dot{\omega}_s - R_s \omega_s$$

$$\tau_r = \theta_{rp} C_{rp}^{-1} - I_r \dot{\omega}_r - R_r \omega_r$$

$$\tau_c - I_c \dot{\omega}_c - R_c \omega_c = \tau_{sp} + \tau_{rp}$$

$$\tau_{rp} \mathrm{TF}_1 = I_p \dot{\omega}_p + R_p \omega_p + \tau_{sp} \mathrm{TF}_2^{-1}$$

According to the motion characteristics of the S-PGT, the torques on the sun gear and ring gear are applied in the same direction. The carrier torque is opposite the sun gear torque.

3.2. Double-Pinion PGT

The double-pinion PGT (D-PGT) has two planetary gear transmissions between the ring and the sun. The kinematic relationship between the D-PGT components is shown in Figure 4. P1 and P2 are planetary gears meshed with the sun gear and the ring gear, respectively. The other symbols are the same as for the S-PGT.

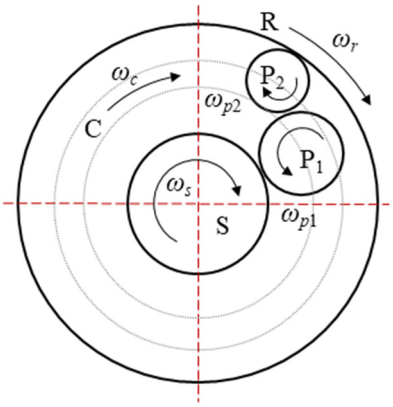

Figure 4. Kinematic diagram of the D-PGT.

The following relationship can be obtained by assuming equal linear velocities at the gear meshing point:

$$\omega_{p1} r_{p1} = (\omega_c - \omega_s) r_s \tag{6}$$

$$\omega_{p2} r_{p2} = (\omega_r - \omega_c) r_c \tag{7}$$

$$\omega_{p1} r_{p1} = \omega_{p2} r_{p2} \tag{8}$$

the characteristic equation is:

$$\omega_s - (1 - \beta)\omega_c - \beta\omega_r = 0 \tag{9}$$

The BG model for the elastic contact in the D-PGT is shown in Figure 5. Node 1 was added to the BG of the S-PGT, to represent an additional planetary gear. Here, θ_{sp} is the relative angular displacement between the planet and the sun, while θ_{rp} is the relative angular displacement between the planet and ring. The parameter θ_p is the relative angular displacement between the two planets.

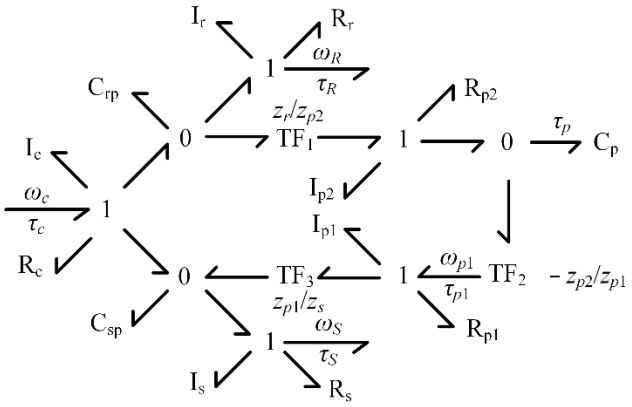

Figure 5. BG model of the D-PGT.

Similarly, the speed and torque equations for the D-PGT can be obtained as follows:

$$\dot{\theta}_{sp} = \omega_c - \omega_r + \mathrm{TF}_3\omega_{p1} \tag{10}$$

$$\dot{\theta}_{rp} = \omega_c - \omega_r - \omega_{p2}\mathrm{TF}_1^{-1} \tag{11}$$

$$\dot{\theta}_p = \omega_{p2} - \omega_{p1} \tag{12}$$

the torque balance equation for the D-PGT is

$$\tau_s = \theta_{sp}C_{sp}^{-1} - I_s\dot{\omega}_s - R_s\omega_s$$

$$\tau_r = \theta_{rp}C_{rp}^{-1} - I_r\dot{\omega}_r - R_r\omega_r$$

$$\tau_c = I_c\dot{\omega}_c + R_c\omega_c + \tau_{sp} + \tau_{rp}$$

$$\tau_p\mathrm{TF}_2^{-1} = \tau_{sp}\mathrm{TF}_3 + I_{p1}\dot{\omega}_{p1} + R_{p1}\omega_{p1}$$

$$\tau_p = \tau_{rp}\mathrm{TF}_1^{-1} - I_{p2}\dot{\omega}_{p2} - R_{p2}\omega_{p2}$$

The power transmission paths for the D-PGT and S-PGT are similar. The difference is that using additional planetary gears changes the direction of the torque acting on the ring gear; for the D-PGT, the torque on the ring gear is opposite in direction to the torque on the sun gear.

Causality is not accounted for by the above two common PGT BG-based models, because a complete transmission system usually adopts a multi-level PGT combination, needs a power source to input power, and requires clutches to cooperate, for realizing the gear-shifting operation. There is no fixed mode for the matching method of a multi-stage PGT with a power source and a clutch. Therefore, the sun gear, the gear ring, and the planet carrier in the PGT are arranged with interfaces that can be connected to the outside, serving as an effort/flow source in BG-based models.

4. The Friction Clutch Model

4.1. The Karnopp Friction Model

The wet friction clutch is an important part of many mechanical transmission systems, such as vehicles, ships, and helicopters. The engagement characteristics of the friction clutch importantly affect the stability of the transmission system [19]. In a more detailed modeling of the clutch, it is usually necessary to consider the oil film hydrodynamic lubrication and the micro-convex elastic contact model. Transmission system studies usually consider the influence of the clutch control mode on the dynamic response.

When a clutch is used in a transmission system, the structural changes of the clutch under the two working conditions of disengagement and engagement directly determine the discontinuity of the structure of the transmission system dynamic model, which makes computer simulations quite challenging [20]. When the clutch is disengaged (that is, $\tau_f = 0$), the driving and driven parts do not affect each other. When the clutch is engaged, under the action of hydraulic pressure $p(t)$, the friction plate and the mating steel plate exhibit the sliding friction, and there is a nonlinear relationship between τ_f, ω_{rel} (relative angular velocities of the driving ω_g and driven ω_d parts) and $p(t)$. When the clutch is engaged, the driving and driven parts are regarded as a fixed connection; τ_f is determined by the external torque T_e, and does not exceed the torque capacity of the clutch T_s. In this case, the relationship between τ_f and ω_{rel} cannot be determined, and a classical method to solve this problem is to replace the friction curve near the zero relative speed with an inclined straight line passing through the origin, which leads to the classical friction model, shown in Figure 6a [7]. However, this method may exhibit numerical stiffness problems, and makes it difficult to solve the system step-by-step using the conventional explicit method; on the other hand, the implicit method can easily deal with this issue.

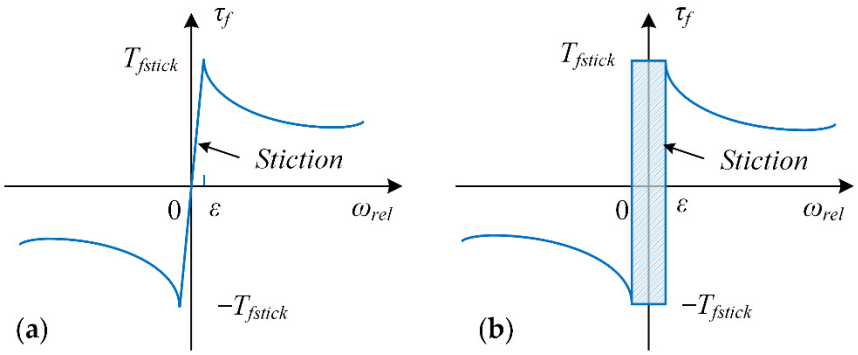

Figure 6. Static friction model: (**a**) classical model, and (**b**) Karnopp model.

The Karnopp model, shown in Figure 6b, can effectively address the above numerical stiffness problem. A small range of $\omega_{rel} = 0$ accessories is defined as $|\varepsilon|$. In this range, τ_f does not depend on ω_{rel}, but only on T_e and T_s. Hence, the Karnopp model can be described as:

$$\tau_f = \begin{cases} T_{fslip} = f(\omega_{rel}, p(t)) & |\omega_{rel}| > \varepsilon \\ T_{fstick} = \begin{cases} T_s \mathrm{sgn}(T_e) & |\omega_{rel}| \le \varepsilon, |T_e| > T_s \\ T_e & |\omega_{rel}| \le \varepsilon, |T_e| \le T_s \end{cases} \end{cases} \tag{13}$$

where the slipping friction function $T_{fslip}(\omega_{rel}, p(t))$. is defined as [21]:

$$T_{fslip} = F_n \mu(t) \mathrm{sgn}(\omega_{rel}) \tag{14}$$

here, F_n represents the positive pressure loaded on the friction plate, while $\mu(t)$ is the dynamic friction coefficient.

$$F_n = N_f \mathrm{A}_p r_e p(t) \tag{15}$$

$$\mu(t) = \mu_c + (\mu_s - \mu_c) \exp\left[-(\omega_{rel}/\omega_s)^{\delta}\right] \tag{16}$$

In the above, N_f is the number of active friction surfaces, A_p is the piston area, r_e is the equivalent clutch radius ($r_e = 2(r_o^3 - r_i^3)/3(r_o^2 - r_i^2)$), μ_c is the Coulomb friction coefficient, μ_s is the static friction coefficient, ω_s is the Stribeck velocity, and δ is the Stribeck shape factor. For $\delta = 1$, the Tustin model [22] is obtained; for $\delta = 2$, the Gauss exponential model [23] is obtained.

4.2. The Friction Model for Hydraulic Clutches

The engagement pressure of a wet multi-disc wet friction clutch is generated by the hydraulic pressure acting on the piston. The characteristics of the engagement pressure directly affect the value of T_{fslip} transmitted by the clutch during the engagement process. Hydraulic loading takes less time than the time for completing the engagement of the clutch. Therefore, in research studies, the hydraulic pressure is typically modeled as a constant or as a linear function [19,24]. However, in practice, the hydraulic loading mode affects T_{fslip}. By fitting the experimental data of actual loads, Wang [25] obtained the functional relationship between the axial outward load and time. In addition, the influence of the loading mode of the exponential curve on the transmission torque was studied [26]. The expressions for the step curve, linear function, and exponential curve are as follows:

$$p_0(t) = P_{\max} \tag{17}$$

$$p_1(t) = aP_{\max}t \tag{18}$$

$$p_2(t) = P_{\max}[1 - \exp(-bt)] \tag{19}$$

where $P_{\max}$ is the maximal bonding pressure, and t is the hydraulic loading time; a and b are some factors. The Karnopp model is shown in Figure 7, and it is based on Equations (13) and (14), respectively.

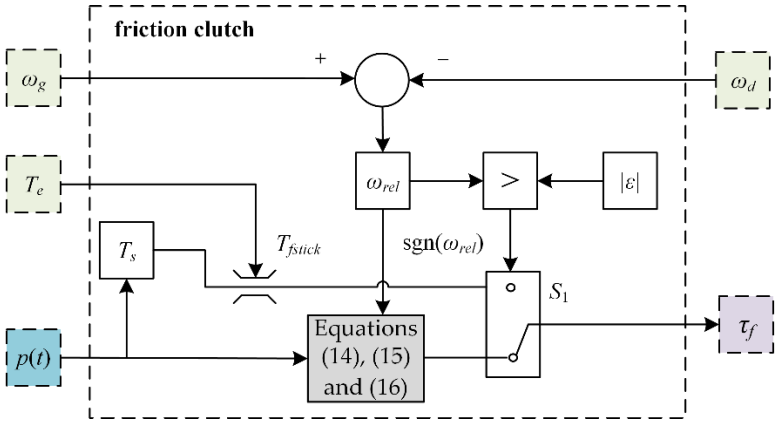

Figure 7. Block diagram of the Karnopp model for hydraulic friction clutches.

Here, ω_g and ω_d are the rotational speeds of the parts in the gear train, τ_f is the torque transmitted by the friction clutch to the gear train, and $p(t)$ is the external excitation of the gearbox, which is controlled by the hydraulic system. To more accurately represent the actual working process of the friction clutch, the model in Figure 7 also includes the following two components: (1) when the hydraulic pressure $p(t) = 0$, $\tau_f = 0$ regardless of the relative speed ω_{rel}; (2) the capacity torque of the friction clutch is $T_s = F_n\mu_s$, and in the static friction state, $T_{\text{stick}} \in [-T_s, T_s]$.

5. The One-Way Clutch Model

A one-way clutch is a mechanical clutch that is mainly composed of an inner ring, a circular array wedge, an outer ring, and a spring. Its structural characteristics prevent it from rotating in one direction, whereas the resistance when rotating in the other direction is negligible [27,28]. To simplify the modeling process, the one-way clutch in the present study was modeled as a nonlinear spring with discontinuous stiffness. The inner ring was simplified as an inertial part without elastic damping, the outer ring was simplified as a grounding part without inertia and elasticity, and the circular array wedge was simplified as a nonlinear elastic damping part without inertia. Accordingly, zero stiffness was assumed in the disengaged state, while a finite linear stiffness was assumed in the engaged state, provided there was relative speed or displacement between the inner and outer parts of the one-way clutch, and provided there was rotational damping. The relative rotation speed [29] or the relative angular displacement [30] between the outer and inner rings could be used for judging the working state. Here, the mathematical model of the one-way clutch was an angular displacement difference model, and the expressions for the torque τ_o of the one-way clutch were as follows:

$$\tau_o = \begin{cases} K_o(\theta_{ir} - \theta_{or}) + C_o\left(\dot{\theta}_{ir} - \dot{\theta}_{or}\right) & \theta_{ir} > \theta_{or} \\ 0 & \theta_{ir} \le \theta_{or} \end{cases} \tag{20}$$

where θ_{ir} is the torsion angle of the inner ring, θ_{or} is the torsion angle of the outer ring, and K_o and C_o are the stiffness and damping, respectively. When the one-way clutch was engaged, the wedges were in close contact with the inner and outer rings. The clearance angle of the clutch during engagement owing to the inertia and edge deformation was ignored. The block diagram of the angular displacement difference model of the one-way clutch is shown in Figure 8.

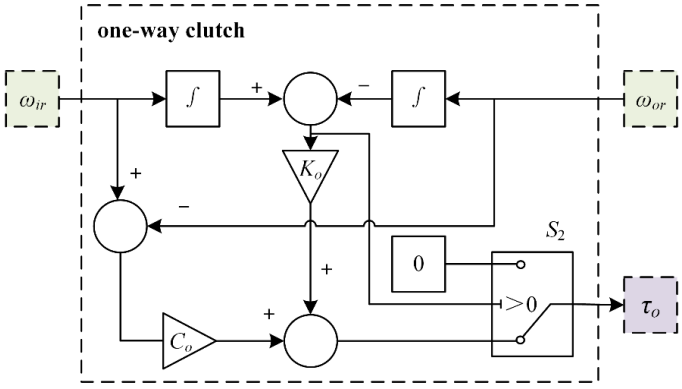

Figure 8. Block diagram of the angular displacement difference model.

In the model, ω_{ir} and ω_{or} are, respectively, regarded as the rotational speed of the parts affixed to the inner ring and the outer ring, respectively, which could be obtained from the gear train model, and τ_o was the torque transmitted by the one-way clutch to the gear train.

6. Coupling the Clutch Models to the PGT Model

Taking the two common PGT models (namely, the friction clutch model and the one-way clutch model) as the basic models, the dynamic model of the transmission can be established by coupling, as shown in Figure 9. However, in actual modeling, it is not easy to obtain the dynamic model directly from the structural diagram (e.g., Figure 1). Therefore, based on the structure and relationships in the diagram, a method for determining the relationships between the basic models is proposed here.

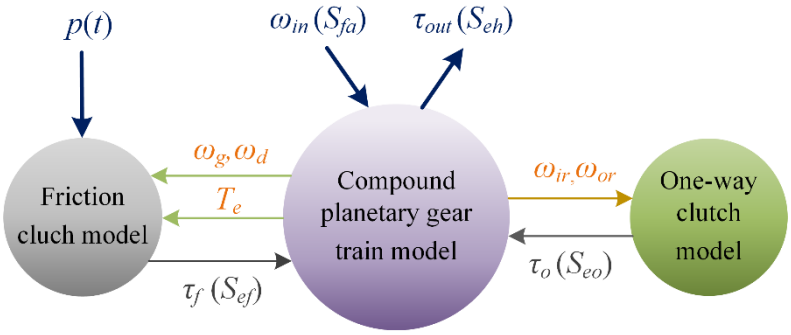

Figure 9. Power transmission relationships among the three basic models.

Step 1. Model of compound PGT

For transmissions with composite PGTs, there are many structural interconnections between PGT elements or members, which can yield different transmission ratios. Taking two individual PGTs as an example, there are six possible structural connections, as listed below: ring gear carrier, sun gear ring gear, sun gear sun gear, carrier–carrier, ring gearing–gear, and sun gear carrier. In addition, there are some special structures, such as connecting the planetary gears of two PGTs, or sharing a ring gear.

Features: The kinematic equation of a composite PGT must be based on the connection mode between the constituting PGTs. The two affixed parts are considered as a whole, and the speed is the same. Each part is represented by node 1, and each meshing point is represented by node 0, considering factors such as the meshing stiffness, rotational damping, and flexibilities of parts. In this way, a dynamic model of a composite PGT is established.

Step 2. Determine the external excitation and output of the gear train.

As shown in Figure 9, the external excitation received by a composite PGT model includes the speed of the input shaft ω_{in}, the load torque of the output shaft τ_{out}, the torque of the friction clutch τ_f, and the torque of the one-way clutch τ_o; T_e, ω_g, and ω_d are transmitted to the wet friction clutch dynamic model; ω_{ir} and ω_{or} are transmitted to the one-way clutch dynamic model.

Features: In addition to the connection ports with the friction clutch and the one-way clutch, each composite PGT has two ports (ω_{in} and τ_{out}).

Step 3. Analyze the input and output of the hydraulic friction clutch.

As shown in Figures 7 and 9, under the hydraulic pressure $p(t)$, the friction clutch starts to work, the friction coefficient $\mu(t)$ is related to ω_g and ω_d in the gear train model, and the sliding friction torque T_{fslip} is transmitted to the gear train. However, when $|\omega_g - \omega_d| \leq \varepsilon$, the friction clutch receives an external torque T_e from the gear train.

Features: There are three connection ports (T_e, ω_g, and ω_d) between each friction clutch and the gear train, as well as an external port ($p(t)$).

Step 4. Connection between the one-way clutch and the transmission system.

It can be seen from Figures 8 and 9 that the one-way clutch is a passively controlled mechanism. Driven by ω_{ir} and ω_{or} in the gear train, the working mode is determined according to the angle difference between the inner and outer rings. When $\theta_{ir} > \theta_{or}$, The torque is transmitted to the gear train. Otherwise, no torque is transmitted.

Features: There are two connection ports (ω_{ir}, ω_{or}) between each one-way clutch and the gear train, and no external ports exist.

The design scenario consists of subjecting the gearbox to an upstream torque that models the torque from the rotor, and a downstream flow source that models the rotational speed imposed by the engine. The hydraulic pressure is applied by the control system. The final multi-system coupled transmission system model is shown in Figure 10.

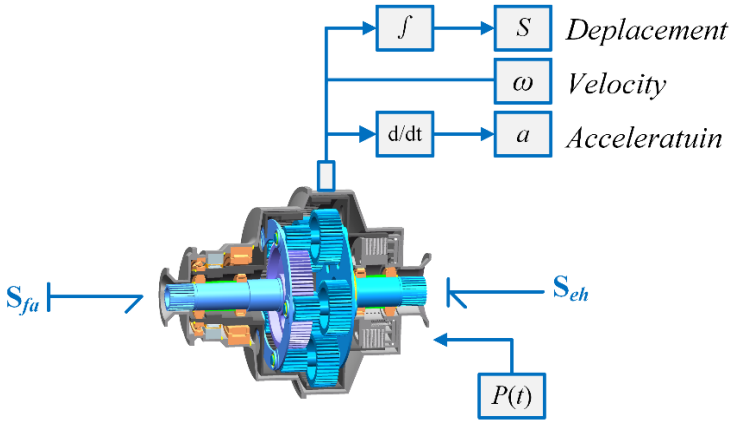

Figure 10. Dynamic design scheme of the transmission system based on the BG model.

7. UncBG Model of a Variable-Speed Gearbox

7.1. Uncertain Factors

There are many sources of uncertainty that cause the vibration response of the gearbox; they may originate from any phase of the task analysis, design, manufacturing, or operation. Taking the helicopter power system as an example, the complete power transmission system is shown in Figure 11. The rotation speed of a typical helicopter rotor is in the order of a few hundred revolutions per minute, whereas the optimal speed of a conventional engine is nearly ten thousand revolutions per minute. At present, the rotor speed of high-speed helicopters needs to be adjusted for meeting the requirements of hovering and high-speed flight. A variable-speed gearbox is usually required for accommodating the two rotational speeds [31], and the realization of this function usually requires the cooperation of the friction clutch and one-way clutch [32,33].

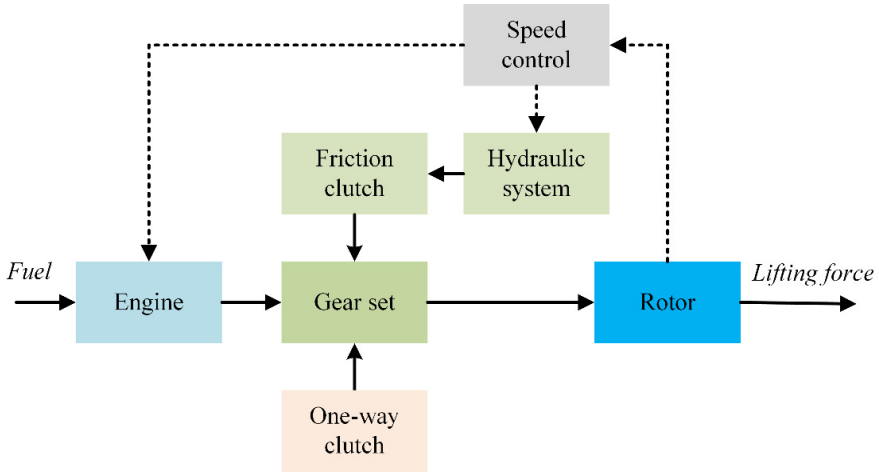

Figure 11. Main subsystems of the helicopter transmission model.

The above analysis reveals that in addition to the uncertain factors such as the gear meshing and tooth surface contact fluctuations at the tooth level in the gearbox, there is also the effect of external excitation, including the engine speed fluctuations, load torque fluctuations, and the aerodynamic torque variation of the rotor. It is worth noting that the transmission system is realized through the hydraulic clutch during the shifting process; thus, the uncertainty of the loading hydraulic fluctuation will also contribute. Finally, the manufacturing errors in the production process of parts, and assembly errors during the gearbox assembly process will directly affect the dynamic characteristics of the transmission system. Therefore, ignoring the uncertainty in a dynamic model will significantly affect the quality and cost of the corresponding transmission system [34].

The time-varying meshing stiffness is the main source of uncertainty in the gear transmission modeling. The meshing phenomenon is responsible for the gearbox noise. In gear transmission, the meshing stiffness changes with time owing to the transition between single- and double-teeth meshing zones, which is related to the geometric and physical characteristics of gear teeth.

The widely used methods for calculating the time-varying meshing stiffness of gears are the Ishikawa deformation formula, the mathematical elasticity method, the ISO standard, and the energy method. In addition, many analytical methods have been developed, especially numerical methods (such as the finite element method), for calculating the meshing stiffness. In this work, the average tooth stiffness was calculated using the formula in the ISO standard. In the process of gear transmission, there is a periodic alternation between the single-tooth and double-tooth meshing states, which leads to regular changes in the gear meshing stiffness. Therefore, the time dependence of the meshing stiffness is expressed by the Fourier series, as follows:

$$k(t) = k_{av} + \sum_{i=1}^{n}(k_{2i}\sin(i\omega t)) = k_{av} + \sum_{i=1}^{n} k_i \cos(i\omega t + \varphi_i) \quad (21)$$

here, k_{av} is the average meshing stiffness; k_i is the ith harmonic amplitude of the stiffness; ω is the meshing frequency; and φ_i is the initial phase of ith harmonic. In addition, $\varphi_i = \arctan(-k_{2i-1}/k_{2i})$, $k_a = \sqrt{k_{2i-1}^2 + k_{2i}^2}$.

The first harmonic term in Equation (21) is taken as the meshing stiffness used for the uncertainty analysis, and Figure 12 shows the meshing stiffness of the involute gear.

$$k(t) = k_{avg} + k_a \cos(\omega t + \varphi_1) \quad (22)$$

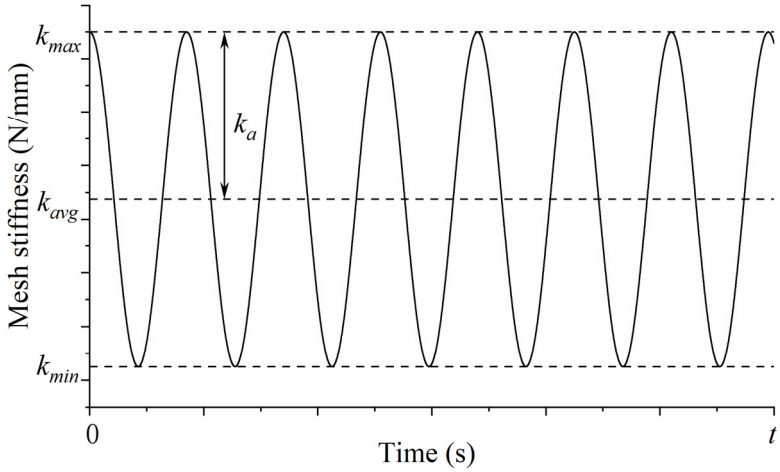

Figure 12. Meshing stiffness of the involute gear.

In this approach, the meshing stiffness values for a single pair of teeth and a double pair of teeth are calculated according to the calculation method of tooth stiffness of the involute gear in the ISO formula draft. The end face coincidence degree is obtained through the geometric parameters and pressure angle of the meshing gear to obtain the average meshing stiffness k_{avg} and stiffness variation amplitude k_a.

The mathematical expression of this stiffness form is relatively simple; it can effectively reflect the influence of the actual meshing stiffness on the system to a certain extent, and is widely used in research studies on gear nonlinear dynamics.

7.2. UncBG Model

The modeling method described above does not consider how uncertainties influence the transmission system's responses, and the obtained coupling dynamic model cannot provide reliable decisions regarding the control system. Uncertain BG (uncBG), which was developed by Kam and Dauphin Tungay [35], can address this problem. Uncertainty in the uncBG model is not suitable for source components, and is mainly used for reconstructing the passive components, for obtaining an invariant linear model with unsteady parameters.

The internal and external excitations were introduced into the uncBG model as follows:

1. The variable rigidity of each C-element in the BG model is considered. In this step, the uncertainty caused by the time-varying meshing stiffness $k(t)$ is introduced into the BG model. Before that, the meshing stiffness in the meshing line direction must be the torsional stiffness in the circumferential direction, which is expressed as follows (where i, j represents a pair of meshing gears, while r_b is the base circle radius):

$$C_{ij}(t) = 1/k_{ij}(t)r_b^2 = 1/\left[k_{ijav} + \bar{k}_{ij1}\cos\left(\omega_{ij}t + \varphi_{ij1}\right)\right]r_b^2 \tag{23}$$

2. According to the structural characteristics of the compound PGT, different fluctuations (0.02–0.05%) are set for each TF element, for simulating the influence of manufacturing and assembly errors on the system's response:

$$\mathrm{TF}' = \begin{cases} \mathrm{TF}_i + 0.005\mathrm{TF}_i\mathrm{randn} & \textit{with uniform load mechanism} \\ \mathrm{TF}_j + 0.002\mathrm{TF}_j\mathrm{randn} & \textit{without uniform load mechanism} \end{cases} \tag{24}$$

3. Considering the speed fluctuation of the engine, a random signal is added to the working speed for simulating uncertain factors; the amplitude of the random signal is set to 0.2% of the working speed:

$$S'_{fa} = S_{fa} + (0.004\mathrm{rand} - 0.002)S_{fa} \tag{25}$$

4. In the form of harmonics, the driving hydraulic pressure of the friction clutch is increased by 2%, to represent the uncertainty of the driving hydraulic pressure (where th is the time at which the hydraulic pressure completes the loading process, and Th is the period of the hydraulic fluctuation):

$$p(t) = \begin{cases} p_i(t) & t \le t_h \\ P_{\max} + 0.02P_{\max}\sin(\frac{2\pi}{T_h}t) & t > t_h \end{cases} (i = 0, 1, 2) \quad (26)$$

The above four methods were introduced into the original BG model (shown in Figure 10), for obtaining the uncBG model, as shown in Figure 13.

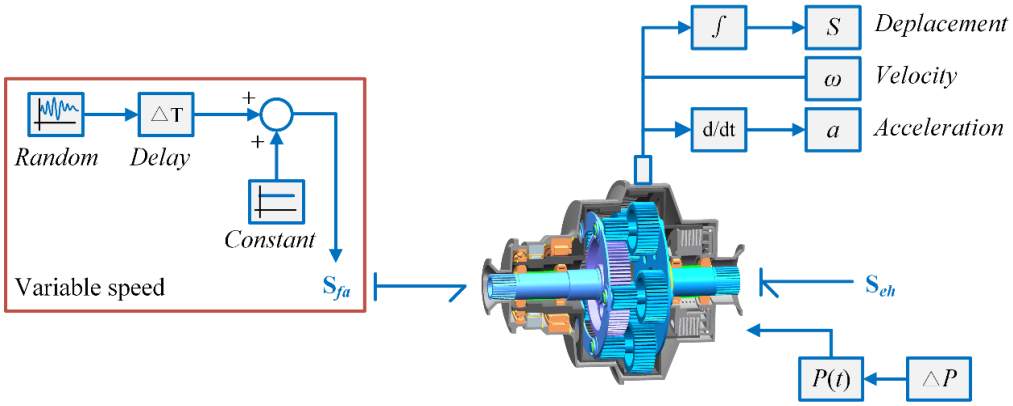

Figure 13. Dynamic design scheme of the transmission system based on the uncBG model.

8. Modeling and Numerical Verification of the Variable-Speed Gearbox

8.1. UncBG Model of a Double-Row Double Planetary Gearbox

According to the power flow path and structural characteristics of the gearbox, different nodes and energy storage elements were set based on the BG theory, and appropriate source elements were selected. Finally, the causal relationship between the nodes and elements was determined. The uncBG model of the gearbox was established, as shown in Figure 14.

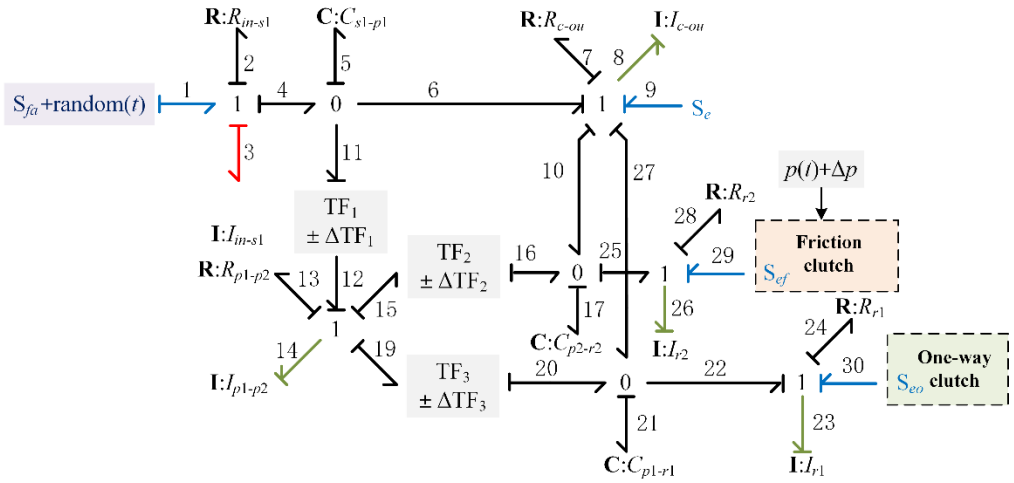

Figure 14. Double-row double planetary uncBG model.

There were three TF elements, corresponding to the three gear meshing points in the gearbox: $TF_1 = r_{p1}/r_s$, $TF_2 = -r_{r2}/r_{p2}$, $TF_3 = -r_{r1}/r_{p1}$. Different meshing points were set to different fluctuation values, according to whether there was a uniform load mechanism: $\Delta TF_1 = 0.005TF_1 \times randn$, $\Delta TF_2 = 0.002TF_2 \times randn$, $\Delta TF_3 = 0.002TF_3 \times randn$.

State variables are physical variables used to characterize the variables of a system with respect to time. The correspondence between mechanical variables and generalized variables is shown in Table 1. The corner marks of the different elements correspond to the number of keys in the bond graph. The differential and algebraic equations can be derived from the uncBG model shown in Figure 14. The friction clutch model and the one-way clutch model are shown in Figures 7 and 8, respectively. An exponential curve was selected for simulating the hydraulic loading characteristics of the friction clutch. The nominal values are listed in Tables 2 and 3.

Table 1. Correspondence between mechanical variables and generalized variables.

Generalized Variables		**Mechanical Variables**	
Meaning	**Symbol**	**Meaning**	**Symbol**
effort variable	e	torque	τ
flow variable	f	angular velocity	ω
generalized displacement	q	angular displacement	θ
generalized momentum	p	moment of inertia	J

Table 2. Compound PGT parameters.

Parameter	**Value**	**Unit**
r_s: Sun base circle radius	108.75	mm
r_{p1}: Planet P1 base circle radius	22.5	mm
r_{p2}: Planet P2 base circle radius	57.35	mm
r_{r1}: Ring R1 base circle radius	153.75	mm
r_{r2}: Ring R2 base circle radius	185	mm
M: modulus	2.5	mm
J_s: Sun inertia	0.0358	kg·m^2
J_p: Panetary inertia	0.0033	kg·m^2
J_{r1}: Ring R1 inertia	0.1825	kg·m^2
J_{r2}: Ring R2 inertia	0.3243	kg·m^2
J_c: Carrier inertia	0.0326	kg·m^2

Table 3. Numerical simulation parameters.

Subsystem	**Parameter**	**Value**	**Unit**
Engine	Input speed S_{fa}	628	rad/s
Rotor	Load torque *Se*	2670/3765.5	Nm
Friction clutch	Hydraulic pressure P_{max}	0.8	MPa
	Exponential curve factor b	14	/
	Number of friction plates N_f	6	/
	Inner radius of friction plate r_i	77.5	mm
	Outer radius of friction plate r_o	110	mm
	Piston cavity area A_p	0.028	m^2
	Dynamic friction coefficient μ_c	0.1	/
	Stribeck coefficient δ	0.02	
	Static friction coefficient μ_s	0.12	/
One-way clutch	Torsional stiffness K_o	2.8×10^5	Nm/rad
	Torsional damping coefficient C_o	0.01	Nm·s/rad

State variable: $\mathrm{X} = \begin{bmatrix} q_5 & p_8 & p_{14} & q_{17} & q_{21} & p_{23} & p_{26} \end{bmatrix}^{\mathrm{T}}$.

Input variable: $\mathrm{U} = \begin{bmatrix} S'_{fa} & S_e & S_{eo} & S_{ef} \end{bmatrix}^{\mathrm{T}}$.

State space equations:

$$\begin{cases} \dot{q}_5 = \omega_{in} - \frac{1}{I_8} p_8 - \mathrm{TF_1}' \frac{1}{I_{14}} p_{14} \\ \dot{p}_8 = \frac{1}{C_5(t)} q_5 - R_7 \frac{1}{I_8} p_8 - \frac{1}{C_{17}(t)} q_{17} - \frac{1}{C_{21}(t)} q_{21} - S_e \\ \dot{p}_{14} = \mathrm{TF_1}' \frac{1}{C_5(t)} q_5 - R_{13} \frac{1}{I_{14}} p_{14} - \frac{1}{\mathrm{TF_2}'} \frac{1}{C_{17}(t)} q_{17} - \frac{1}{\mathrm{TF_3}'} \frac{1}{C_{21}(t)} q_{21} \\ \dot{q}_{17} = \frac{1}{I_8} p_8 + \frac{1}{\mathrm{TF_2}'} \frac{1}{I_{14}} p_{14} - \frac{1}{I_{26}} p_{26} \\ \dot{q}_{21} = \frac{1}{I_8} p_8 + \frac{1}{\mathrm{TF_3}'} \frac{1}{I_{14}} p_{14} - \frac{1}{I_{23}} p_{23} \\ \dot{p}_{23} = \frac{1}{C_{21}(t)} q_{21} - R_{24} \frac{1}{I_{23}} p_{23} + S_{eo} \\ \dot{p}_{26} = \frac{1}{C_{17}(t)} q_{17} - R_{28} \frac{1}{I_{26}} p_{26} + S_{ef}(p(t)) \end{cases} \quad (27)$$

On expressing the abovementioned differential Equation (27) with state space equations for matrices and vectors, we obtain:

$$\dot{X} = AX + BU \quad (28)$$

Here, A is a seven-order matrix containing all the coefficients of the state variable on the right-hand side of Equation (27). B is the matrix comprising the coefficients of the input variable on the right-hand side of Equation (27).

The derived mathematical model is a multi-energy domain shift dynamics model with uncertain factors, including mechanical energy and hydraulic energy, involving uncertain factors such as input random signal, driving hydraulic fluctuation, time-varying meshing stiffness, and comprehensive error.

A mathematical model based on the bond graph model was established in MATLAB, and specific parameters adopted in the simulation are presented in Tables 2 and 3. Figure 15a shows the shift dynamics simulation scheme of the double-row double planetary gearbox. Based on Figure 14 and Equation (27), the Simulink scheme of the compound planetary train based on the bond graph was obtained, as shown in Figure 15b, and the Runge–Kutta method was used to solve the shift model.

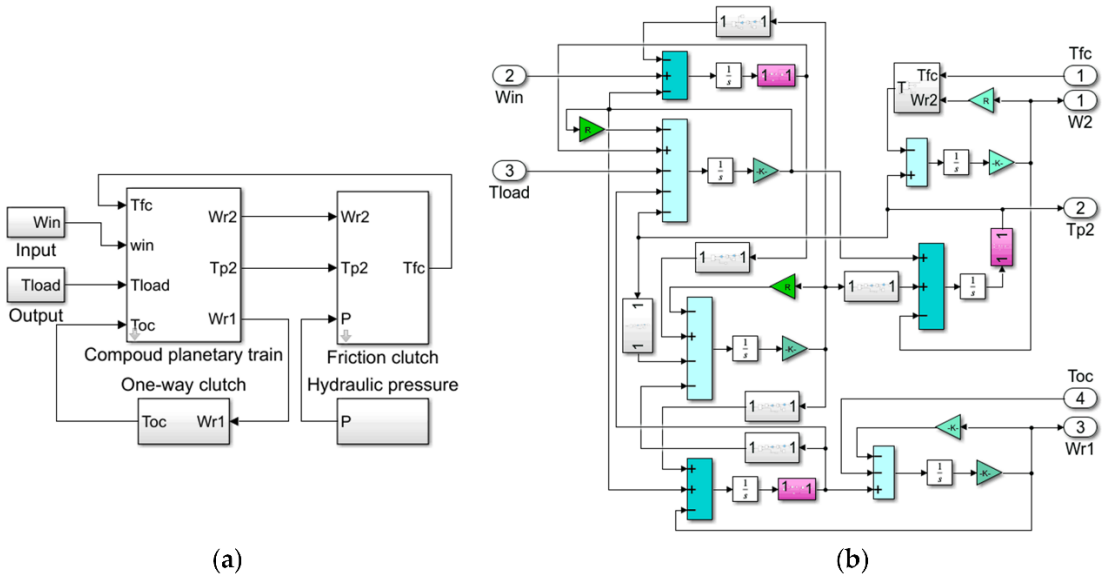

Figure 15. Simulation scheme using MATLAB Simulink: (**a**) double-row double planetary gearbox shift model, (**b**) compound planetary train.

8.2. Results and Discussion

The simulation results are shown in Figures 16 and 17, respectively. Figure 16 shows the rotating speeds of the output shaft, planetary gear, ring gear R1, and ring gear R2. Before and after gear shifting, the average rotating speeds of the output shaft were 260

and 366 rad/s respectively, with fluctuations of 6 and 2.5%, and the transmission ratio was 2.42 and 1.42 respectively; The rotating speeds of the planetary gears were 1779 and 1264 rad/s respectively, with fluctuations of 2.5 and 1.7%. The average rotating speeds of the ring gear R1 were 0.1 and 182 rad/s respectively, and the average rotating speeds of ring gear R2 were 256 and 0.001 rad/s respectively. During the gear-shifting process, different parts exhibit different dynamic responses of speed increase or deceleration. The steady-state values of output shaft, planetary gear, ring gear R1, and ring gear R2 rotating speed were close to the theoretical values. The deviation between the two gear transmission ratios obtained by simulation and the design value is within 5.8%, and rotating speed of each part is continuous during the shift process. The above analysis results show that shows the correctness of the uncBG model of the gearbox and the continuity of the shift process simulation. Figure 17 shows the angular acceleration of the output shaft, planetary gear, ring gear R1, and ring gear R2. Obviously, the angular acceleration of the planetary gear varies the most. In the actual gearbox, the planetary gear rotates at a high speed while rotating with the carrier; therefore, the vibration is obvious, and the theoretical results of the uncBG model are in agreement with the actual situation. Theoretically, ring gear R1 is affixed before shifting, but the simulation results show that there is angular acceleration, which may be related to the uncertain factors and the model of the one-way clutch. Theoretically, ring gear R1 rotates freely before shifting, and is affixed after shifting. The simulation results in Figure 17 show that ring gear R1 has acceleration before shifting while the acceleration is zero after shifting, which is consistent with the theoretical analysis results.

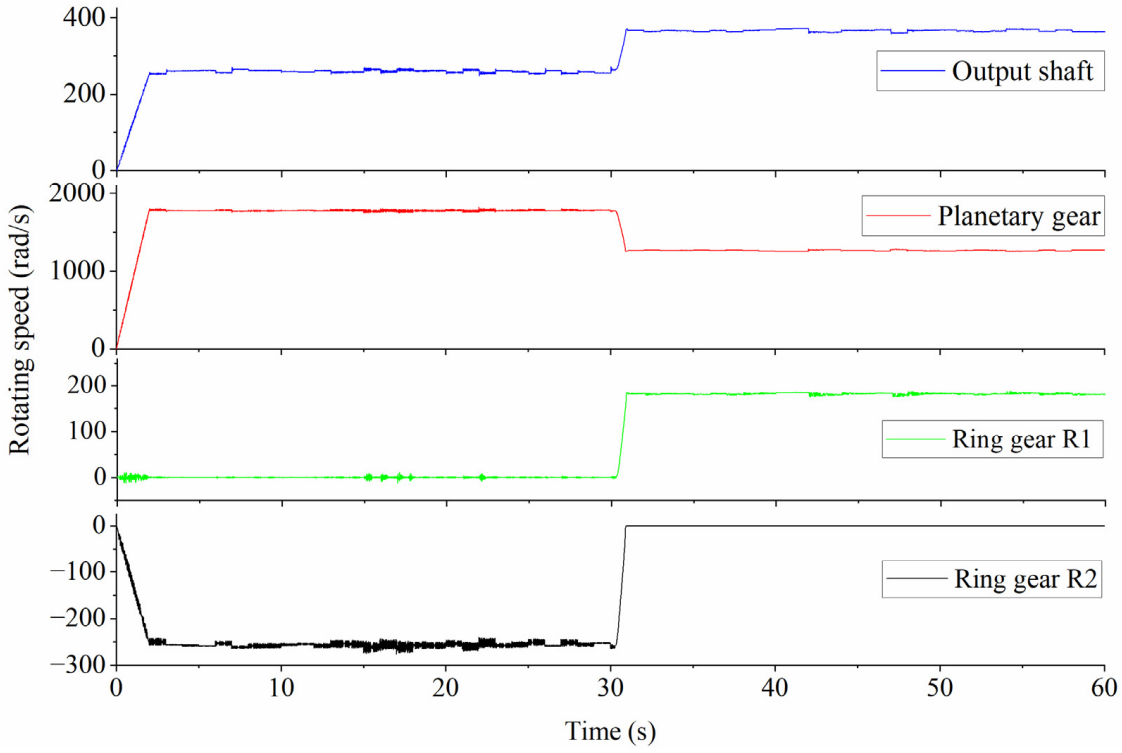

Figure 16. Waveforms of the output shaft, planetary gear, ring gear R1, and ring gear R2 rotating speeds.

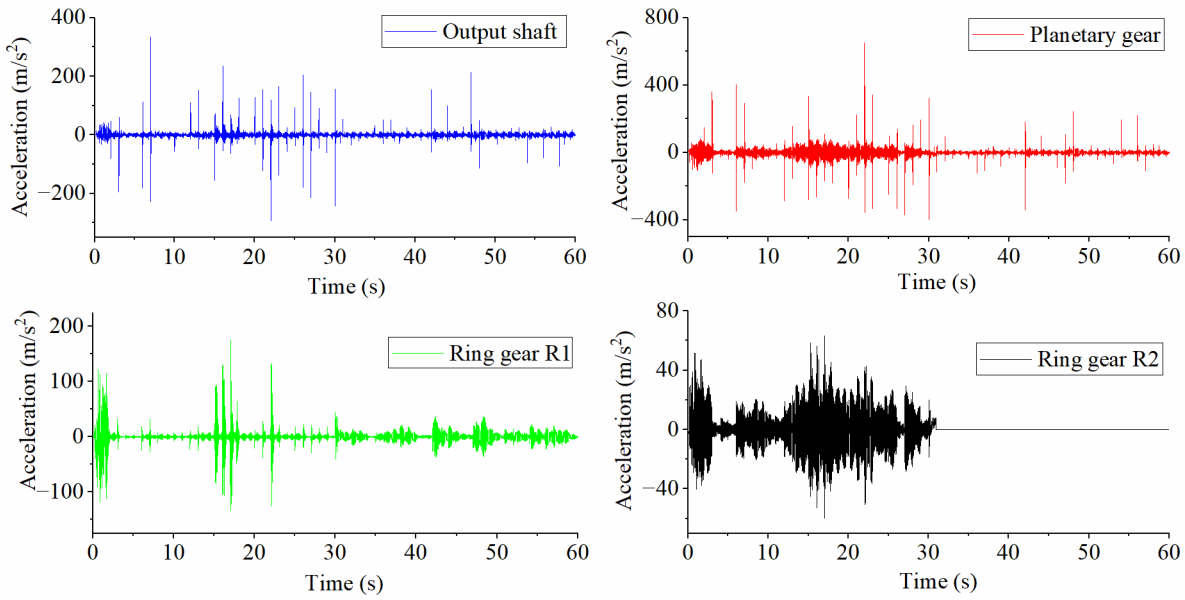

Figure 17. Waveforms of the output shaft, planetary gear, ring gear R1, and ring gear R2 angular accelerations.

9. Conclusions

According to the structural characteristics of the variable-speed gearbox, the dynamic relationships between the main functional components were decoupled, and the basic models of the composite PGT, friction clutch, and one-way clutch were constructed. The standardized modeling process of the BG model was developed and presented based on the kinematic and dynamic relationships between the system's components; a modular rapid modeling and analysis method applicable to this type of gearbox was obtained, which can simulate the gearbox shifting process, containing multiple energy domains with a continuous model and solving the problem that the conventional physical equations cannot be continuously simulated in the complex integrated variable speed gearbox shifting process. Meanwhile, various uncertainties, such as errors (design, manufacture, and assembly errors), time-varying stiffness, input speed variations, and hydraulic fluctuations were introduced into the BG model, yielding the uncBG model. As demonstrated with the example of a double-row double planetary gearbox, the uncBG method was effective for the dynamic modeling of a gearbox. Furthermore, it will likely facilitate the shift dynamics analysis, control strategy design, and other related research.

Author Contributions: Data curation, W.T.; Methodology, Y.Z.; Validation, S.L.; Writing—original draft, J.W.; Writing—review & editing, H.Y. All authors have read and agreed to the published version of the manuscript.

Funding: This work is supported by the National Natural Science Foundation of China (Grant No. 52075552).

Conflicts of Interest: The authors declare no conflict of interest.

References

1. Borutzky, W. *Bond Graph Methodology: Development and Analysis of Multidisciplinary Dynamic System Models*; Springer Science and Business Media: London, UK, 2010.
2. Yao, W.; Chen, X.; Luo, W.; Van Tooren, M.; Guo, J. Review of uncertainty-based multidisciplinary design optimization methods for aerospace vehicles. *Progr. Aeronaut. Sci.* **2011**, *47*, 450–479. [CrossRef]
3. Drewniak, J.; Kopeć, J.; Zawiślak, S. Graph models of automobile gears-kinematics. *Int. J. Appl. Mech. Eng.* **2014**, *19*, 563–573. [CrossRef]
4. Deur, J.; Ivanović, V.; Assadian, F.; Kuang, M.; Tseng, E.H.; Hrovat, D. Bond graph modeling of automotive transmissions and drivelines. *IFAC Proc.* **2012**, *45*, 427–432. [CrossRef]

5. Vangheluwe, H.; Lara, J.D.; Mosterman, P.J. An introduction to multi-paradigm modelling and simulation. In Proceedings of the 2002 AI, Simulation and Planning in High Autonomy Systems conference (AIS'2002), Lisboa, Portugal, 7–10 April 2002; pp. 9–20.
6. Boudon, B.; Malburet, F.; Carmona, J.C. Simulation of a helicopter's main gearbox semiactive suspension with bond graphs. *Multibody Syst. Dyn.* **2017**, *40*, 375–405. [CrossRef]
7. Barjuei, E.S.; Toxiri, S.; Medrano-Cerda, G.A.; Caldwell, D.G.; Ortiz, J. Bond Graph Modeling of An Exoskeleton Actuator. In Proceedings of the 10th Computer Science and Electronic Engineering (CEEC 2018), Colchester, UK, 19–21 September 2018; pp. 101–106. [CrossRef]
8. Deur, J.; Asgari, J.; Hrovat, D. Modeling of an automotive planetary gear set based on karnopp model for clutch friction. In Proceedings of the ASME 2003 International Mechanical Engineering Congress and Exposition (IMECE 2003), Washington, DC, USA, 15–21 November 2003; pp. 903–910. [CrossRef]
9. Deur, J.; Asgari, J.; Hrovat, D.; Kovač, P. Modeling and analysis of automatic transmission engagement dynamics-linear case. *J. Dyn. Syst. Meas. Control.* **2006**, *128*, 263–277. [CrossRef]
10. Deur, J.; Asgari, J.; Hrovat, D.; Kovač, P. Modeling and analysis of automatic transmission engagement dynamics-nonlinear case. *J. Dyn. Syst. Meas. Control.* **2006**, *128*, 251–262. [CrossRef]
11. Ranogajec, V.; Deur, J.; Coric, M. Bond graph analysis of automatic transmission shifts including potential of extra clutch control. *SAE Int. J. Engines.* **2016**, *9*, 1929–1945. [CrossRef]
12. Ivanovic, V.; Tseng, H.E. Bond graph based approach for modeling of automatic transmission dynamics. *SAE Int. J. Engines* **2017**, *10*, 1999–2014. [CrossRef]
13. Ranogajec, V.; Ivanović, V.; Deur, J.; Tseng, H.E. Optimization-based assessment of automatic transmission double-transition shift controls. *Control Eng. Pract.* **2018**, *76*, 155–166. [CrossRef]
14. Liu, J.; Yu, L.; Zeng, Q.; Li, Q. Synthesis of multi-row and multi-speed planetary gear mechanism for automatic transmission. *Mech. Mach. Theor.* **2018**, *128*, 616–627. [CrossRef]
15. Li, X.T.; Wang, A.L. A modularization method of dynamic system modeling for multiple planetary gear trains transmission gearbox. *Mech. Mach. Theor.* **2019**, *136*, 162–177. [CrossRef]
16. Jouilel, N.; Radouani, M.; El Fahime, B. Wind Turbine's Gearbox Aided Design Approach Using Bond Graph Methodology and Monte Carlo Simulation. *Int. J. Precis. Eng. Manuf. Green Technol.* **2021**, *8*, 89–101. [CrossRef]
17. Mir-Haidari, S.E.; Behdinan, K. On the vibration transfer path analysis of aero-engines using bond graph theory. *Aerosp. Sci. Technol.* **2019**, *95*, 105516. [CrossRef]
18. Tan, W.Z.; Wu, J.M.; Ni, D.; Yan, H.Z.; Xiang, E.M.; Liu, S.Q. Dynamic modeling and simulation of double-planetary gearbox based on bond graph. *Math. Probl. Eng.* **2021**, *2021*, 3964808. [CrossRef]
19. Bao, H.Y.; Huang, W.; Lu, F.X. Investigation of engagement characteristics of a multi-disc wet friction clutch. *Tribol. Int.* **2021**, *159*, 106940. [CrossRef]
20. Montazeri-Gh, M.; Miran Fashandi, S.A. Modeling and simulation of a two-shaft gas turbine propulsion system containing a frictional plate–Type clutch. *Proc. Inst. Mech. Eng. M J. Eng. Marit. Environ.* **2019**, *233*, 502–514. [CrossRef]
21. Karnopp, D.C. Computer simulation of stick-slip friction in mechanical dynamic systems. *J. Dyn. Syst. Meas. Control.* **1985**, *107*, 100–103. [CrossRef]
22. Tustin, A. The effects of backlash and of speed dependent friction on the stability of closed-cycle control systems. *J. Inst. Electr. Eng. IIA Autom. Regul. Servo Mech.* **1974**, *94*, 143–151. [CrossRef]
23. Armstrong-Helouvry, B. Stick-slip arising from Stribeck friction. *Proc. ICRA* **1990**, *2*, 1377–1382. [CrossRef]
24. Iqbal, S.; Al-Bender, F.; Ompusunggu, A.P.; Pluymers, B.; Desmet, W. Modeling and analysis of wet friction clutch engagement dynamics. *Mech. Syst. Signal Process.* **2015**, *60–61*, 420–436. [CrossRef]
25. Wang, Y.; Li, Y.; Liu, Y.; Zhang, W. Modeling and experimental research on engaging characteristics of wet clutch. *Ind. Lubr. Tribol.* **2019**, *71*, 94–101. [CrossRef]
26. Natsumeda, S.; Miyoshi, T. Numerical simulation of engagement of paper based wet clutch facing. *J. Tribol.* **1994**, *116*, 232–237. [CrossRef]
27. Liu, Z.H.; Yan, H.Z.; Cao, Y.M.; Lai, Y. Bifurcation and chaos analysis of the spur gear transmission system for one-way clutch, two-shaft assembly. *Shock Vib.* **2017**, *2017*, 8621514. [CrossRef]
28. Ke, Z.; Wei, W.; Liu, C. The dynamic wedging and friction characteristics of one-way clutch under transient loads from stator. *Tribol. Int.* **2020**, *152*, 106568. [CrossRef]
29. Mockensturm, E.M.; Balaji, R. Piece-wise linear dynamic systems with one-way clutches. *J. Vib. Acoust.* **2005**, *127*, 475–482. [CrossRef]
30. Ding, H. Periodic responses of a pulley–belt system with one-way clutch under inertia excitation. *J. Sound Vib.* **2015**, *353*, 308–326. [CrossRef]
31. Snyder, C.A.; Robuck, M.; Wilkerson, J.; Nordstrom, C. Summary of the large civil tiltrotor (LCTR2) engine gearbox study. In Proceedings of the International Power Lift Conference 2010, Proceedings of the International Power Lift Conference 2010, Philadelphia, PA, USA, 5–7 October 2010; pp. 416–431.
32. Stevens, M.A.; Lewicki, D.G.; Handschuh, R.F. Concepts for multi-speed rotorcraft drive system—Status of design and testing at NASA GRC. In Proceedings of the American Helicopter Society (AHS) 71st Annual Forum, Virginia Beach, VI, USA, 5–7 May 2015.

33. Stevens, M.A.; Handschuh, R.F.; Lewicki, D.G. Offset Compound Gear Inline Two-Speed Drive. U.S. Patent 8,091,445, 10 January 2012.
34. Jawad, A.; Dantan, J.; Sabri, V.; Beaucaire, P.; Gayton, N. A statistical tolerance analysis approach for over-constrained mechanism based on optimization and Monte Carlo simulation. *Comput. Aid. Des.* **2012**, *44*, 132–142. [CrossRef]
35. Kam, C.S.; Dauphin-Tanguy, G. Bond graph models of structured parameter uncertainties. *J. Franklin Inst.* **2005**, *342*, 379–399. [CrossRef]